
Morphological Study of Proto-Planetary Nebulae Since APN III

Toshiya Ueta

Department of Physics and Astronomy, University of Denver,
2112 E. Wesley Ave., Denver, CO 80208, U.S.A. tueta@du.edu

Summary. Morphological study of proto-planetary nebulae has been the workhorse to understand the critical phases mass loss along the asymptotic giant branch and the initial shaping that take place in their circumstellar envelopes. After recapping the motivation of the study and earlier development prior to APN III, I will highlight some of the initiatives that have contributed in the field since APN III.

Key words: planetary nebulae: general – reflection nebulae – stars : AGB and post-AGB – stars : mass loss – stars: winds, outflows

1 PPN Morphology Primer

Proto-planetary nebulae (PPNe) usually refer to the circumstellar envelopes (CSEs) associated with post-asymptotic giant branch (post-AGB) stars. The post-AGB phase is a brief transitional phase of the stellar evolution lasting only on the order of 10^3 yr beyond the tip of the AGB and prior to the onset of photoionization at the beginning of the planetary nebula (PN) phase [13, 36].

Fig. 1 shows an evolutionary track (red line) of a $2 M_{\odot}$ solar metallicity star from the main sequence to the white dwarf phase [10], together with representative images of an AGB star, a PPN and a PN (respectively from top right to top left), illustrating how the CSE structure develops as the central star evolves. The AGB CSEs are largely taken as synonymous with spherical symmetry [9], while PNe are known to have developed structures far more than spherically symmetric [1]. PPNe are found to have developed at least axisymmetric CSE structures [19, 28]. Thus, non-spherical CSE structures must arise sometime during the late AGB phase. However, we have not understood exactly when and how stars manage to do so. The immediate objectives of the PPN morphological study is, therefore, to obtain clues as to how AGB and post-AGB stars manage to shape their CSEs through mass loss.

There is a fundamental distinction between PPNe and PNe that determines the way these objects are best probed. While PNe are emission nebulae containing ionized gas, PPNe are reflection nebulae consisting of dust and neutral gas. Hence, PPN morphological study in the optical would provide only an *indirect* glimpse of the dust distributions via scattered star light, which is susceptible to self-extinction.

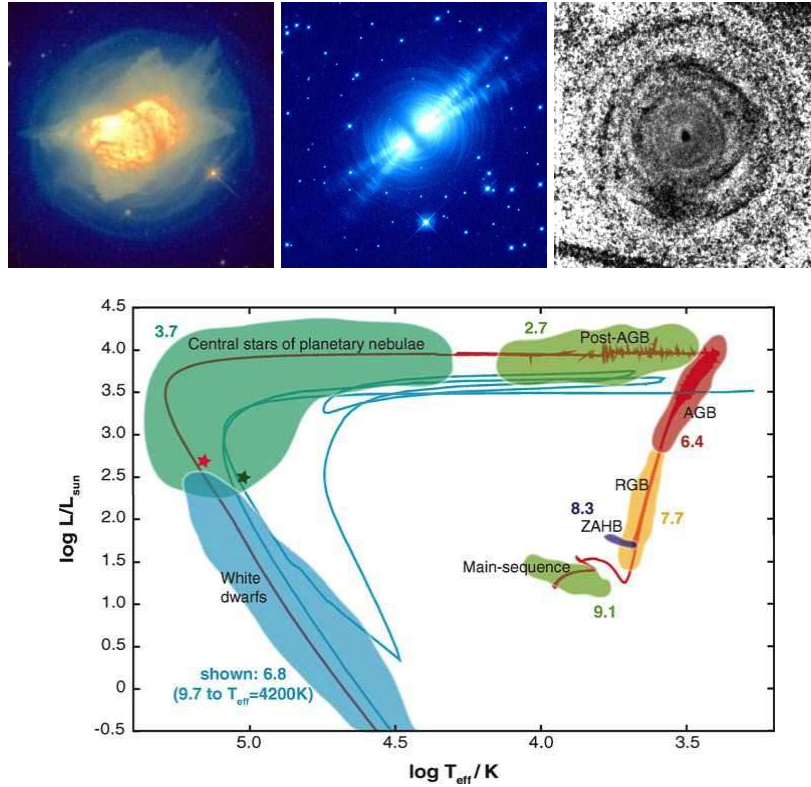


Fig. 1. **Top Left:** an HST optical/IR composite image of NGC 7027, a PN, showing a variety of structures [4, 16]. **Top Middle:** an HST optical image of the Egg Nebula, a PPN, displaying its well-defined bipolar structure [23]. **Top Right:** a ground-based $B+V$ image of IRC +10 216, an AGB star, exhibiting spherical shells [18]. **Bottom:** a complete evolutionary track (red line) of a $2 M_{\odot}$ star [10].

Instead, thermal IR would provide a *direct* probe of the dust distribution. Therefore, PPN morphologies are best investigated by using *both* means at the highest spatial resolution. (Probing the molecular component is beyond the scope of this review [2].)

2 Before APN III

Prior to APN II, WFPC2 and NICMOS on-board HST and ground-based mid-IR array instruments became available. HST observations of PPNe started to reveal spectacular bipolar nebulosities in a number of observations [14, 23]. Then, it was typically assumed that PPNe are intrinsically bipolar and elliptical PPNe are simply those oriented pole-on.

However, subsequent PPN observing campaigns in the mid-IR uncovered that some optically elliptical PPNe possessed an edge-on dust torus within their reflection

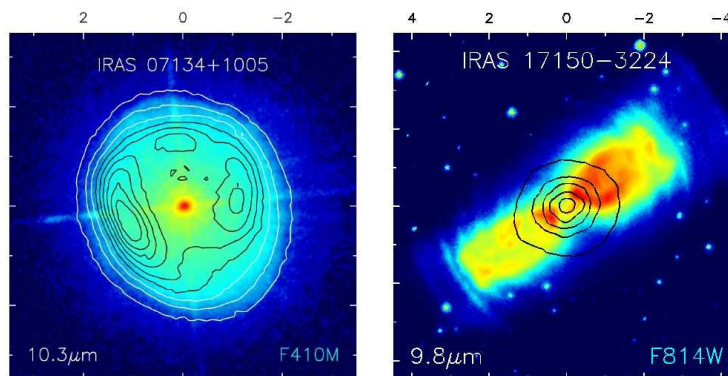


Fig. 2. Two types of PPNe revealed by a combined optical/mid-IR survey [19, 20, 28]. **Left:** IRAS 07134+1005 (HD 56126) harbors an optically thin, edge-on dust torus (two mid-IR peaks representing the limb-brightened edges) within an elongated reflection nebula. **Right:** IRAS 17150-3224 has an optically thick dust torus that appears as a “dust lane” between the optical bipolar lobes. HST data are in color and mid-IR data in contours. Tickmarks are offsets from the central star in arcsec.

nebulae [19, 29]. Fig. 2 (left) shows an optically elliptical PPN IRAS 07134+1005 in color. In the inclination angle context, this PPN has to be close to pole-on. Yet, its mid-IR data in contours indicate that there is an edge-on dust torus because these two emission peaks represent the limb-brightened edges of an edge-on torus, in which the line of sight optical depth is the highest. In this case, the optical depth of the torus is low enough that the dust torus would not appear as a dust lane between two bipolar lobes as in the case of the optically thicker, IRAS 17150-3224 (Fig. 2, right).

By APN III, enough observational evidence and supporting dust radiative transfer modeling results were accumulated to conclude that (1) two physically distinct kinds (optically thin and thick) of PPNe exist, (2) equatorial density enhancement is present in both types and (3) the optical depth of the shell determines the morphology [20, 28, 30].

3 After APN III

3.1 Coming of Natural/Laser Guide Star Adaptive Optics Systems

There have been a number of new techniques/methods that improve our ability to investigate PPN morphologies in detail. The first is adaptive optics (AO) imaging with a natural and laser guide star (NGS and LGS, respectively). Fig. 3 shows a set of $2\ \mu\text{m}$ images of the Egg Nebula, with (left, LGSAO at Keck) and without (right, NICMOS on HST): the LGSAO image achieves higher resolution and a wider dynamical range *from the ground*.

Such NGS/LGS AO images allow us to examine not only the overall CSE structures but also local structures within the CSEs. The corkscrew structure have been

recognized within the bipolar lobes of IRAS 16342-3814, suggesting the presence of some precessing agent carving the inner walls of the lobes [24]. The bipolar lobes in PPNe appear to be well-defined, close-ended cavities as in IRAS 18276-1431 [26]. AO data have strengthened the case for the presence of some precessing agent to generate the bipolar structure in PPNe. However, the equatorial density enhancement in the CSEs (the source of the “dust lane”) does not appear to be causing this precession. Rather, the enhancement seems to predate the onset of the bipolar structure generation.

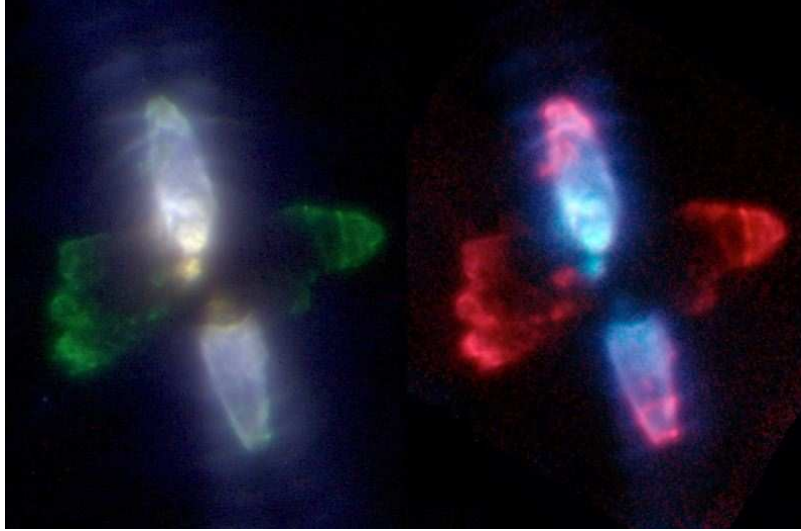


Fig. 3. The Egg Nebula at $2 \mu\text{m}$ with and without AO. **Left:** a Keck/LGSAO (H , H_2 and K_{cont}) image [17]. **Right:** an HST/NICMOS (H_2 and $2.15 \mu\text{m}$) image [22].

3.2 Imaging Polarimetry

The second example is the use of imaging polarimetry. The structure of elliptical (optically thin) PPNe is difficult to study because the central star is usually so bright that the structure gets washed out by the enormous central star. Imaging polarimetry permits us to separate the polarized component (scattered by dust in the CSE) and the unpolarized component (direct star light) [7, 8], helping to overcome this difficulty.

Fig. 4 shows the total intensity map (left), polarized intensity map (middle) and polarized strength map (right) of IRAS 07134+1005 at $2 \mu\text{m}$ [31]. Although the total intensity map looks almost identical to an optical map (Fig. 2, left, in color), the polarized intensity map reveals the equatorially enhanced structure in detail while the polarized strength maps reveals the hollow nature of the CSE. The structure of bipolar PPNe has also been investigated by the method to learn more about the structures in the lobes [33].

PPNe as reflection nebulae appear to be limb-brightened cavities in the middle of the AGB CSEs that are intrinsically equatorially enhanced. The compressed edge

of the cavities seems to show the density gradient in the azimuthal direction in both PPN types. In bipolar PPNe, however, the azimuthal gradient is often accompanied by a pitch angle that makes the CSE structure appear corkscrew-like.

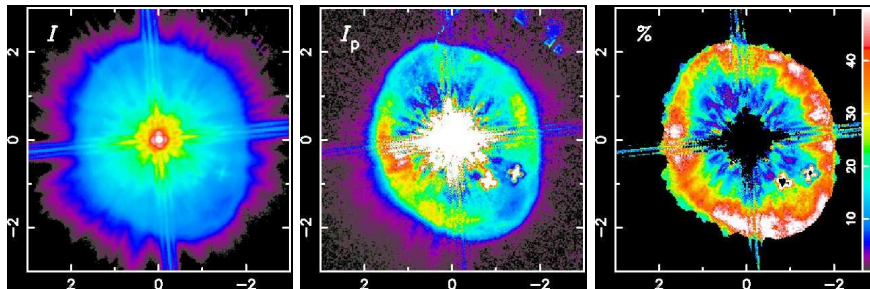


Fig. 4. Imaging Polarimetry on IRAS 07134+1005 [31]. **Left:** a $2\ \mu\text{m}$ total intensity map. **Middle:** a polarized intensity map. **Right:** a polarization strength map. Tickmarks show offsets from the central star in arcsec.

3.3 More Optical/Mid-IR Surveys

HST have accumulated an enormous wealth of optical imaging data of PPNe (more than 80% of known PPNe have been imaged to date). There have been at least two new compilations based on these results [25, 27].

One study follows the previous SOLE versus DUPLEX dichotomy scheme (Fig. 5, left), and confirms the division between them and their being both ends of the optical depth spectrum, i.e., SOLE and DUPLEX being optically thin and thick equatorially enhanced CSEs, respectively [27]. This study also indicates that PPN candidates lacking reflection nebulae may be SOLE objects close to pole-on.

While this multi-wavelength (optical+mid-IR) approach has been very effective to obtain the complete picture of the PPN structures, the amount of mid-IR data has not increased as much as the optical data. It is partly because of the intrinsically compact nature of PPNe, which works against the intrinsically larger diffraction limit in the mid-IR, and of comparably lesser availability of mid-IR array instruments. Nevertheless, thermal IR imaging of PPNe is an avenue of research that must be pursued as it would yield much-needed *direct* clues for the dust distribution in PPNe.

Another study attempts to devise a more detailed classification scheme (Fig. 5, right). This classification is detailed enough to describe most/all of the observed PPN features [25]. However, it is unclear if the differences among these morphological classes necessarily corresponds to the differences among physical CSE properties. Since PPNe are reflection nebulae, the CSEs of *the same physical structure* can result in *very distinct morphologies* depending on the optical depth of these CSEs. Optical PPN morphologies yield at most *indirect* clues for the CSE structures. To obtain the complete picture of the PPN structures, *direct* clues for the CSE structures, through methods that directly probe the dust distribution in the CSEs, are also necessary. This is why a multi-wavelength approach has been effective.

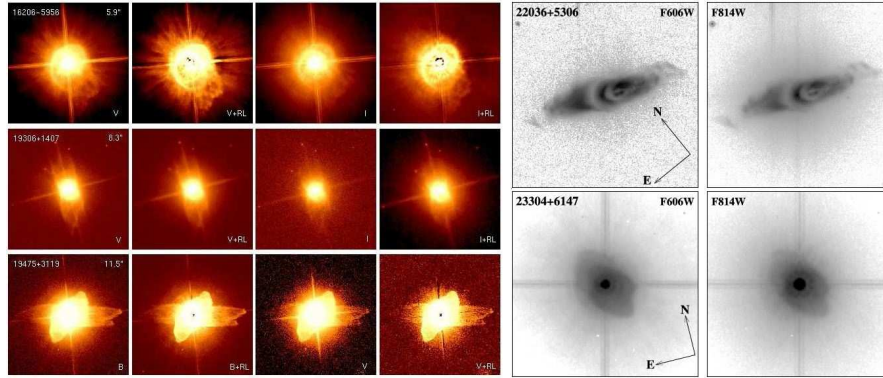


Fig. 5. Images from two new compilations of imaging survey data. **Left:** Siódmiak et al. following the SOLE versus DUPLEX dichotomy [27]. **Right:** Sahai et al. devising a detailed classification of PPN morphologies of reflection nebulae.

3.4 Interferometry

While AO systems enable sub- $0.1''$ spatial resolution imaging in the optical/near-IR, it is still not enough to resolve the inner CSE structures of compact sources in cases dust grains condense near the sublimation temperature (typically at tens of mas). Optical/IR interferometry has been becoming a viable alternative technique. In general, interferometric observations are finding flattened over-density regions with a rather significant scale height in the innermost regions of PPNe, which are consistent with the overall PPN structures. Further details are deferred to discussion by Chesneau [3] and Deroo [5] in this volume.

3.5 Molecular Hydrogen

H_2 emission at $2.12 \mu\text{m}$ has been an important probe of PPNe because it can yield much needed velocity information in the CSEs in spite of the limiting Gatley's rule stating that H_2 emitting objects are exclusively bipolar [12]. Nevertheless, H_2 emission has been shown to arise from the ends of the lobes due to collisional shocks, suggesting the presence of collimated fast outflows carving asymmetry in the lobes relatively early in the PPN phase [11, 35].

3.6 Far-IR Observations

While we have learned more details on the PPN structures and some clues for the shaping, we have not figured out exactly when and how the non-spherical shaping of the CSE commences. One can either observe “younger” objects that are in the process or “older” objects whose CSEs show the transformation as the far-IR surface brightness distribution. The latter has become a possibility thanks to new far-IR opportunities provided by *Spitzer* and *AKARI* [6, 32, 34]. When the data are fully analyzed we will gain more insights on AGB mass loss at earlier epochs.

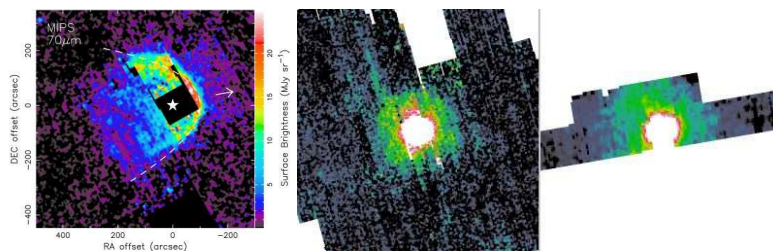


Fig. 6. **Left:** the interface between the AGB wind and interstellar medium around R Hya seen by *Spitzer* [32]. **Middle & Right:** the extended CSE around U Ant at 70 μm (middle) and 160 μm (right), in which earlier mass loss history is imprinted.

4 Summary and Beyond APN IV

Two major findings since APN III thus seem to be (1) (confirmation of) the presence of the equatorial density enhancement predating the era of detailed PPN shaping and (2) recurring indications for the presence of collimated outflows and some precessing agent in bipolar PPNe. These will be obvious items to follow-up beyond APN IV.

In the optical front, HST/WFC3 and maturing AO techniques (and perhaps closure-phase optical/near-IR interferometry) will serve our purposes well. In the thermal IR front, we will have more opportunities with *Herschel* and *SOFIA* while we may have to wait until the era of *JWST* to make substantial progress in the mid-IR. The use of multi-wavelength (thermal dust emission + dust-scattered light) approach exploiting these new opportunities will continue to yield a better, more complete picture of the PPN structures and enhance our understanding of the PPN shaping and AGB mass loss in time for APN V.

References

1. B. Balick, A. Frank: *ARA&A*, 40, 439–486 (2002)
2. A. Castro-Carrizo: In: this volume
3. O. Chesneau, et al: In: this volume
4. R. Ciardullo, H.E. Bond, M.S. Sipior, L.K. Fullton, C.-Y. Zhang, K.G. Schaefer: *AJ*, 118, 488–508 (1999)
5. P. Deroo, et al: In: this volume
6. T. Do, M. Morris, R. Sahai, K. Stapelfeldt: *AJ*, 134, 1419–1431 (2007)
7. T. M. Gledhill, A. Chrysostomou, J.H. Hough, J.A. Yates: *MNRAS*, 322, 321–342 (2001)
8. T. M. Gledhill *MNRAS*, 356, 883–898 (2005)
9. H. Habing, J.A.D.L. Blommaert: Carbon and Oxygen-Rich Progenitors of Planetary Nebulae. In: *IAU Symp. 155: Planetary Nebulae*, ed by R. Weinberger, A. Acker (Kluwer, Dordrecht 1993) p 243
10. F. Herwig: *ARA&A*, 43, 435–479 (2005)
11. B.J. Hrivnak, D.M. Kelly, K.Y.L. Su, S. Kwok, R. Sahai: *ApJ*, 650, 237–245 (2006)
12. J.H. Kastner, D.A. Weintraub, I. Gatley, K.M. Merrill, R.G. Probst: *ApJ*, 462, 777–785 (1996)
13. S. Kwok: *ARA&A*, 31, 63–92 (1993)
14. S. Kwok, K.Y.L. Su, B.J. Hrivnak: *ApJL*, 501, 117–121 (1998)
15. S. Kwok, K. Volk, B.J. Hrivnak, *ApJ*, 573, 720–727 (2002)
16. W.B. Latter, A. Dayal, J.H. Bieging, C. Meakin, J.L. Hora, D.M. Kelly, A.G.G.M. Tielens: *ApJ*, 539, 783–793 (2000)
17. D. Le Mignant, et al: In: this volume
18. N. Mauron, P.J. Huggins: *A&A*, 349, 203–208 (1999)
19. M. Meixner, et al: *ApJS*, 122, 221–242 (1999)
20. M. Meixner, T. Ueta, M. Bobrowsky, A.K. Speck: *ApJ*, 571, 936–946 (2002)
21. C. Muthumariappan, S. Kwok, K. Volk: *ApJ*, 640, 353–359 (2006)
22. R. Sahai, et al: *ApJL*, 492, 163–167 (1998a)
23. R. Sahai, et al: *ApJ*, 493, 301–311 (1998b)
24. R. Sahai, D. Le Mignant, C. Sánchez Contreras, R.D. Campbell, F.H. Chaffee: *ApJL*, 622, 53–56 (2005)
25. R. Sahai, M. Morris, C. Sánchez Contreras, M. Claussen: *AJ*, submitted (2007)
26. C. Sánchez Contreras, D. Le Mignant, R. Sahai, A. Gil de Paz, M. Morris: *ApJ*, 656, 1150–1166 (2007)
27. N. Siódmiak, M. Meixner, T. Ueta, B.E.K. Sugerman, G.C. Van de Steene, R. Szczerba: *AJ*, submitted (2007)
28. T. Ueta, M. Meixner, M. Bobrowsky: *ApJ*, 528, 861–884 (2000)
29. T. Ueta, et al: *ApJ*, 557, 831–843 (2001)
30. T. Ueta, M. Meixner: *ApJ*, 586, 1338–1355 (2003)
31. T. Ueta, K. Murakawa, M. Meixner: *AJ*, 129, 1625–1641 (2005)
32. T. Ueta, et al: *ApJL*, 648, 39–42 (2006)
33. T. Ueta, K. Murakawa, M. Meixner: *AJ*, 133, 1345–1360 (2007)
34. T. Ueta, et al: In: this volume
35. G.C. Van de Steene, T. Ueta, P.A.M. van Hoof, M. Reyniers, A.G. Ginsburg: In: this volume
36. H. Van Winckel: *ARA&A*, 41, 397–427 (2003)